

Facile synthesis of hybrid graphene and carbon nanotubes as a metal-free electrocatalyst with active dual interfaces for efficient oxygen reduction reaction†

Cite this: *J. Mater. Chem. A*, 2013, **1**, 9603

Received 28th June 2013
Accepted 3rd July 2013

DOI: 10.1039/c3ta12520c

www.rsc.org/MaterialsA

Jang-Soo Lee,^{‡,a} Kiyoung Jo,^{‡,b} Taemin Lee,^a Taeyeong Yun,^a Jaephil Cho^{*a}
and Byeong-Su Kim^{*a}

We report metal-free electrocatalysts to enhance utilization of dissolved and gaseous oxygen during oxygen reduction reaction (ORR). Proper balance between hydrophobicity and hydrophilicity is achieved using reduced graphene oxide (rGO) and polyelectrolyte functionalized multiwalled carbon nanotubes (pMWNTs). In this unique architecture, both two- and three-phase reactions in ORR can be maximized with a quasi-four-electron pathway.

Oxygen reduction is a vital reaction for energy conversion systems in which oxygen can be used as the cathode active material.¹ Since oxygen undergoes a reduction process with high overpotential in both acidic and alkaline media, the electrocatalyst to facilitate the oxygen reduction reaction (ORR) is significant. In particular, compared to its behavior in acidic media, the ORR in an alkaline environment is more facile and can be catalyzed by a broader range of materials.^{2–4} For that reason, the development of efficient ORR electrocatalysts is essential for improving electrochemical performance of alkaline fuel cells and metal–air batteries.^{5–8} In general, the utilization of oxygen at the cathode interface for the three-phase (*i.e.* catalyst (solid), electrolyte (liquid), and oxygen (gas)) reaction should be improved.⁹ Furthermore, despite its relatively low efficiency, two-phase ORR, involving dissolved oxygen, also needs to be considered particularly for the design of high-performance metal-free electrocatalysts.⁹ With its unique structures to alleviate the mass transport effect, it maximizes the utilization of available gas phase and dissolved oxygen. It

leads to our key idea of developing more efficient electrocatalysts to maximize both gaseous and dissolved oxygen involved during the ORR through the appropriate combination of hydrophobicity and hydrophilicity. In order to realize this design principle, it is critical to balance the hydrophilic and hydrophobic properties of catalysts for a large number of active reaction sites to participate. For this purpose, we suggest a unique model system which can offer insight into the importance of dual interfaces by using hybrid nanomaterials.

Although many noble metal catalysts, such as Pt and Pt-based alloys, have been employed as ORR catalysts with excellent efficiency, the high cost and poor long-term durability intrinsically associated with the Pt group ORR catalysts have restricted their use for large-scale applications.^{8,10–17} The recent development of non-precious metal-based or metal-free catalysts for effective ORR has thus generated considerable interest.^{18–30} In particular, metal-free nitrogen-doped carbon materials have been demonstrated to exhibit good electrocatalytic activities for ORR which are comparable to commercial Pt/C (see Table S1 in the ESI†).^{18,20,28,31–33} The design of many of these metal-free electrocatalysts, however, mainly focused on the electronic interaction between oxygen and carbon materials doped by heteroatoms or adsorbed with polyelectrolytes without addressing the phase boundary structures of electrocatalysts within the electrode. Herein, a unique design for the synthesis of 3D-metal-free electrocatalysts by controlled hybridization of one-dimensional (1D) multiwalled carbon nanotubes (MWNTs) and two-dimensional (2D) reduced graphene oxide (rGO) nanosheets is reported. Specifically, we combined poly(diallyldimethylammonium chloride) (PDAC)-functionalized hydrophobic MWNTs (pMWNTs) with hydrophilic rGO nanosheets having a large surface area for the construction of metal-free carbon electrocatalysts to allow effective oxygen access in both gas and aqueous forms (Fig. 1).

In a typical experiment, we dispersed the hydrophobic MWNTs in an aqueous solution of PDAC with NaCl by sonication (see the Experimental section in the ESI†). The filtered suspension of pMWNTs exhibited good colloidal stability with a

^aInterdisciplinary School of Green Energy, Ulsan National Institute of Science and Technology (UNIST), Ulsan 689-798, Korea. E-mail: jpcho@unist.ac.kr; bskim19@unist.ac.kr

^bSchool of Natural Sciences, Ulsan National Institute of Science and Technology (UNIST), Ulsan 689-798, Korea

† Electronic supplementary information (ESI) available: Preparation and characterization of hybrid rGO/pMWNT catalysts, as-prepared samples of thin films for contact angle measurements, and a detailed method for R(R)DE experiments. See DOI: 10.1039/c3ta12520c

‡ These authors contributed equally to this work.

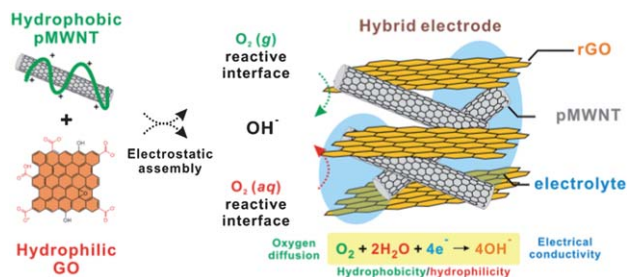


Fig. 1 Schematic representation of a randomly stacked 3D hybrid structure of polyelectrolyte functionalized multiwalled carbon nanotubes (pMWNTs) with reduced graphene oxide (rGO) nanosheets.

zeta-potential of +29.9 mV, which is constant over the entire pH range tested (pH 3–11). This confirms the presence of a positively charged strong polyelectrolyte PDAC coating layer on pMWNTs. High-resolution X-ray photoelectron spectroscopy (XPS) and FT-IR measurements further supported the successful adsorption of PDAC chains onto the MWNTs (see Fig. S1 and S2 in the ESI†). In particular, the intermolecular charge transfer from MWNTs to electron-deficient quaternary ammonium nitrogen atoms of the adsorbed PDAC was evident from the negative shift of the N1s peak from 402 (pure PDAC) to 401.5 eV (pMWNTs) (see Fig. S3 in the ESI†).^{34,35} Consistent with the XPS results, Raman spectroscopy also revealed the charge transfer effect needed to enhance ORR activities of the hybrid rGO/pMWNTs. As reported previously, the up-shift of G bands from 1594.2 cm⁻¹ in pMWNTs to 1588.6 cm⁻¹ in rGO/pMWNT_(10:1) illustrated the charge transfer between rGO and pMWNTs. Concomitantly, the I_D/I_G ratio increased from 1.14 for pMWNTs to 1.35 for rGO/pMWNT_(0.5:1) and even to 1.49 for rGO/pMWNT_(10:1), indicating the presence of disordered graphitic structures in the hybrid electrocatalysts (see Fig. S4 in the ESI†). This partial positive charge developed along the backbone of pMWNTs is known to play a key role in regulating the oxygen adsorption modes and in facilitating electron transfer for enhanced ORR activity.^{28,35} Using the prepared stable suspension of pMWNTs, we started preparing hybrid electrodes by mixing pMWNTs with the GO suspension generated by employing the modified Hummers method (typically, ratios of GO/pMWNTs = 0.5–10).^{36–38} After the hybrid nanostructures were formed *via* electrostatic interactions between the two oppositely charged constituent components, the GO was subsequently reduced to rGO using the reducing agent hydrazine to restore structural pathways to transport charges needed for ORR.^{39–41} The excess hydrazine and unbound free PDAC were then removed by filtration, followed by extensive rinsing. The resulting hybrid electrocatalysts of rGO/pMWNTs with varying ratios were readily redispersed in water and remained stable without any noticeable aggregation for several months (see Fig. S5 in the ESI†). It should be noted that the rGO was additionally functionalized with PDAC as a control.

The structure and morphology of rGO/pMWNTs were examined by scanning electron microscopy (SEM) and transmission electron microscopy (TEM). The representative SEM image revealed 3D interconnected network structures of

pMWNTs with interdispersed rGO nanosheets driven from electrostatic stacking between oppositely charged carbon nanomaterials (Fig. 2a). The TEM image further validated the thin layer of graphene sheet stacked with pMWNTs (Fig. 2b). Furthermore, it was found that thin films of pMWNTs and rGO showed the sessile contact angles of 125° and 70.3°, respectively, while their hybrid rGO/pMWNT_(0.5:1) exhibited an intermediate value of 84.5° (Fig. 2c–e). These results show that our unique hybrid composite has dual interfaces that can balance the hydrophobic and hydrophilic nature for efficiently catalyzing ORR using both gaseous and dissolved oxygen molecules.

By measuring the average number of electrons transferred (n_{avg}) per oxygen molecule derived from the slope of the Koutecký–Levich plot (i^{-1} vs. $\omega^{-0.5}$) (Fig. 3a),^{18,35,42} we first explored the optimization of the rGO/pMWNT ratio (see also Fig. S6 in the ESI†). As can be seen in Fig. 3a, the ORR activity was considerably affected by the relative amounts of pMWNTs and rGO within the hybrids. While pMWNTs provided the majority of the catalytic active sites due to their hydrophobic nature and the induced partial positive charge on their surface, introduction of rGO into their hybrid materials also improves the utility of both dissolved and gaseous oxygen and facilitates electron transfer during ORR due to its hydrophilic nature. Interestingly, however, pure pMWNTs without rGO displayed significantly lower ORR activity similar to that of pure rGO. Among all samples investigated in this study, rGO/pMWNT_(0.5:1) demonstrated the highest n_{avg} value of 3.6 ± 0.40 for an efficient one-step, quasi-four-electron process.

To gain further insight into the ORR activity of hybrid rGO/pMWNTs, we performed linear sweep voltammetry (LSV) measurements using a rotating ring-disk electrode (RRDE) in O₂-saturated electrolyte solution of 0.1 M KOH, which revealed that ORR at the hybrid rGO/pMWNT_(0.5:1) electrode exhibited a relatively high limiting current density and more positive onset potential with respect to its single-component counterparts (*i.e.*, rGO and pMWNTs) (Fig. 3b). For example, the limiting current density of the hybrid rGO/pMWNT_(0.5:1) electrode at -0.8 V reached -5.0 mA cm⁻², whereas the corresponding values for

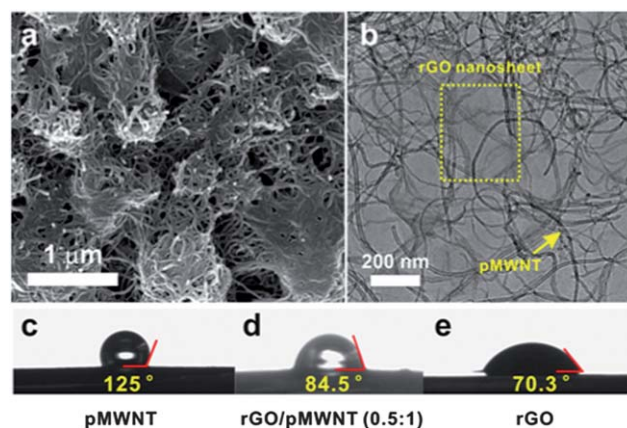


Fig. 2 Representative (a) SEM and (b) TEM images of rGO/pMWNT_(0.5:1). (c–e) Contact angle images of a water droplet on (c) pMWNT, (d) rGO/pMWNT_(0.5:1), and (e) rGO films.

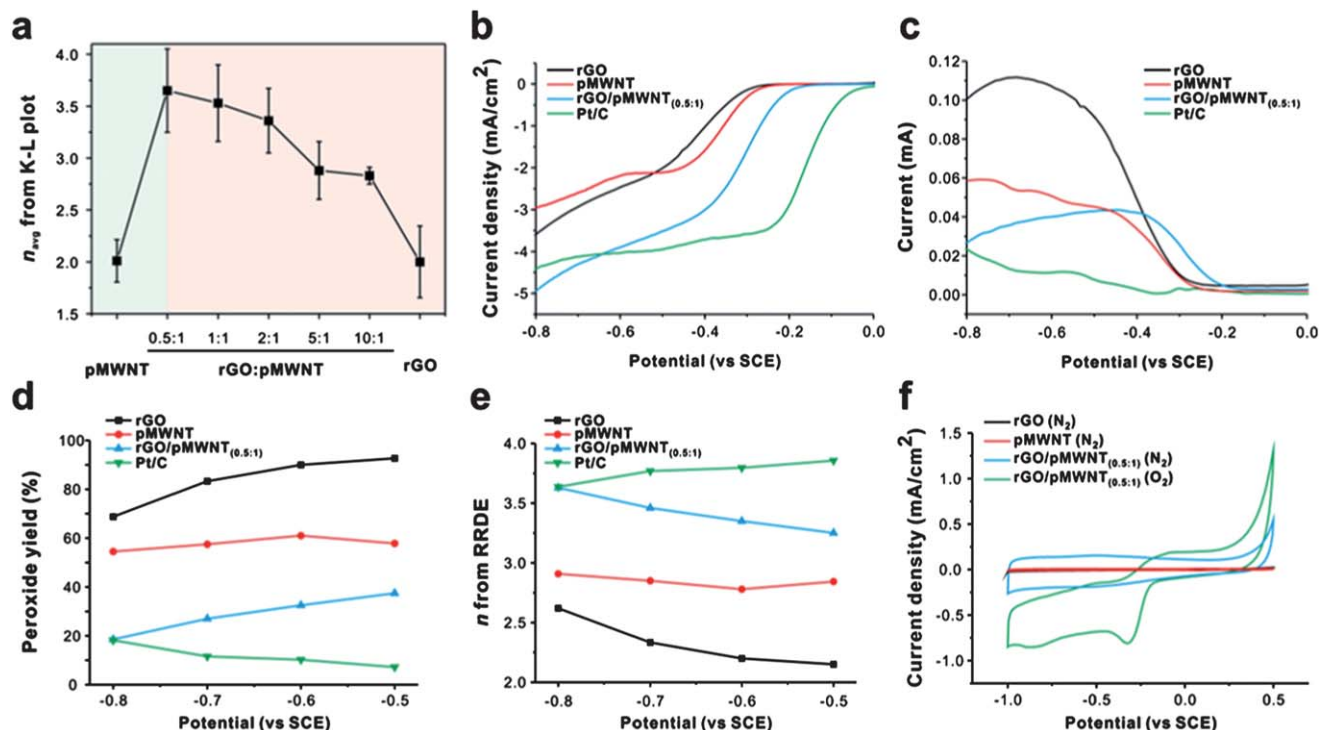


Fig. 3 (a) Average number of electrons (n_{avg}) transferred per O_2 molecule at different rGO/pMWNT ratios, measured at -0.4 , -0.5 , and -0.6 V using the Koutecky–Levich plot. A comparison with control sets of pMWNTs and rGO is also presented. (b–e) Steady-state RRDE experiments of pMWNTs, rGO, hybrid rGO/pMWNT_(0.5:1) and Pt/C, respectively, in O_2 -saturated 0.1 M KOH at 2000 rpm. (b) Disk current density and (c) ring current were separated for convenience. (d) Peroxide yields (%) and (e) the number of electrons (n) transferred from as-prepared samples. (f) CV curves of pMWNTs, rGO, and hybrid rGO/pMWNT_(0.5:1) in N_2 - and O_2 -saturated 0.1 M aqueous KOH electrolyte solution at a scan rate of 50 mV s^{-1} .

the rGO and pMWNT electrodes were -3.6 and -3.0 mA cm^{-2} , respectively. In addition, the onset potential of the rGO/pMWNT electrode up-shifted considerably toward -0.23 V compared to those of rGO (-0.35 V) and pMWNTs (-0.32 V) at a constant current density of -0.5 mA cm^{-2} .

Further, the superior catalytic activity of the hybrid rGO/pMWNT_(0.5:1) over that of the respective single-component was also confirmed by the hydrogen peroxide yields (%) and the number of electrons (n) transferred during the ORR, as determined from disk and ring currents (Fig. 3b and c). In particular, the number of electrons transferred was measured to be 3.3–3.6 (very close to 3.6 in Fig. 3a) for the hybrid rGO/pMWNT_(0.5:1), suggesting that it is an efficient 4-electron transfer pathway with its peroxide yield of $\sim 25\%$ at -0.75 V (Fig. 3d and e). Furthermore, it is noteworthy that the current density of the hybrid rGO/pMWNT_(0.5:1) was even slightly higher than that of Pt/C catalysts in high overpotential regions; this observation indicates that more active sites could participate in ORR due to its unique architecture which can facilitate both aqueous and gaseous oxygen transport to active sites. Though it was fabricated *via* an extremely facile way, these results demonstrate that the catalytic activity of this hybrid rGO/pMWNT_(0.5:1) is comparable to that of other metal-free catalysts which were synthesized through harsh treatments in an alkaline solution (see Table S1 in the ESI†). The high ORR activity of the hybrid resulted from the proper balance of hydrophilicity and

hydrophobicity and the unique catalyst structures of the dual interface. The significance of the dual interface was further confirmed by evaluating its charge per loading which is proportional to active surface area by measuring non-faradaic current under inert N_2 conditions (Fig. 3f). In this study, we chose measuring total charges of unit mass instead of BET because the dual interfaces of gaseous and dissolved oxygen species involved during mixed phase ORR can be better addressed with this method. The charge per unit loading was 2.66 C g^{-1} for rGO, 2.16 C g^{-1} for pMWNTs and 62.9 C g^{-1} for rGO/pMWNT_(0.5:1), respectively. As expected, rGO/pMWNT_(0.5:1) had about 30 times higher surface area than those of pMWNTs and rGO, clearly supporting that a fine hydrophobic–hydrophilic balance was established in the hybrid electrode, which resulted in an increase in the active surface area by facilitating the access of the electrolyte and dissolved and gaseous oxygen. Taken together, with the above physio-chemical and electrochemical analyses, it is reasonable to conclude that factors more crucial than simple charge transfer play a role in improving ORR activities of the 3D hybrid rGO/pMWNT electrocatalysts. Further, the rational design of the hydrophobic and hydrophilic dual interfaces within the hybrid electrode is critical to optimize the catalytic activity for reducing gaseous and dissolved oxygen at the electrode.

Finally, in order to evaluate the advantages of hybrid carbon-based electrochemical catalysts over conventional Pt-based

electrocatalysts for potential practical applications, current-time chronoamperometric response was used to examine the methanol crossover effect and long-term stability. No crossover effect was observed in the hybrid rGO/pMWNT_(0.5:1) composite upon the addition of 3.0 M methanol, while Pt/C showed a sharp current decrease under identical conditions (see Fig. S7 in the ESI†). The chronoamperometric durability response for 20 000 s verified that the hybrid rGO/pMWNT_(0.5:1) exhibited very slow attenuation with a high current retention of 61%, a value higher than that of Pt/C (see Fig. S8 in the ESI†).

Conclusions

In conclusion, we have developed electrostatic force driven randomly stacked three-dimensional hybrid electrocatalysts to maximize the utility of oxygen during the oxygen reduction reaction (ORR). The newly developed carbon electrodes formed using multiwalled carbon nanotubes hybridized with reduced graphene oxide nanosheets exhibited a remarkably enhanced ORR activity without extreme conditions for synthesis. The observed improvement in the ORR performance can be attributed to the increased number of active reaction sites and to enhanced mass transport associated with the well-established hydrophobic and hydrophilic dual interfaces and the porosity within the electrode. The high catalytic activity combined with the extremely facile synthetic nature of this electrocatalyst with dual interface active sites makes its development an important step forward in designing and utilizing carbon nanomaterials in electrocatalysts, and opens up new possibilities for carbon materials to be used as alternative cost-effective catalysts for metal-air batteries and alkaline fuel cells.

Acknowledgements

This work was supported by the next generation secondary battery R&D program of MKE/KEIT[H0301-12-1009], and also by the National Research Foundation of Korea (NRF) grant (2012R1A1A2040782).

Notes and references

- J. S. Lee, S. Tai Kim, R. Cao, N. S. Choi, M. Liu, K. T. Lee and J. Cho, *Adv. Energy Mater.*, 2011, **1**, 34–50.
- B. B. Blizanac, P. N. Ross and N. M. Markovic, *Electrochim. Acta*, 2007, **52**, 2264–2271.
- E. Antolini and E. R. Gonzalez, *J. Power Sources*, 2010, **195**, 3431–3450.
- Y. Liang, H. Wang, J. Zhou, Y. Li, J. Wang, T. Regier and H. Dai, *J. Am. Chem. Soc.*, 2012, **134**, 3517–3523.
- J.-S. Lee, G. S. Park, S. T. Kim, M. Liu and J. Cho, *Angew. Chem., Int. Ed.*, 2013, **52**, 1026–1030.
- J. Zhang, M. B. Vukmirovic, Y. Xu, M. Mavrikakis and R. R. Adzic, *Angew. Chem., Int. Ed.*, 2005, **44**, 2132–2135.
- B. C. Steele and A. Heinzl, *Nature*, 2001, **414**, 345–352.
- V. R. Stamenkovic, B. Fowler, B. S. Mun, G. Wang, P. N. Ross, C. A. Lucas and N. M. Marković, *Science*, 2007, **315**, 493–497.
- R. Cao, J. S. Lee, M. Liu and J. Cho, *Adv. Energy Mater.*, 2012, **2**, 816–829.
- Z. Chen, M. Waje, W. Li and Y. Yan, *Angew. Chem., Int. Ed.*, 2007, **46**, 4060–4063.
- M. Winter and R. J. Brodd, *Chem. Rev.*, 2004, **104**, 4245–4269.
- V. Di Noto, E. Negro, S. Polizzi, F. Agresti and G. A. Giffin, *ChemSusChem*, 2012, **5**, 2451–2459.
- V. Di Noto, E. Negro, K. Vezzù, L. Toniolo and G. Pace, *Electrochim. Acta*, 2011, **57**, 257–269.
- Z. Peng and H. Yang, *J. Am. Chem. Soc.*, 2009, **131**, 7542–7543.
- M.-H. Shao, K. Sasaki and R. R. Adzic, *J. Am. Chem. Soc.*, 2006, **128**, 3526–3527.
- L. Xiao, L. Zhuang, Y. Liu and J. Lu, *J. Am. Chem. Soc.*, 2008, **131**, 602–608.
- B. Lim, M. Jiang, P. H. Camargo, E. C. Cho, J. Tao, X. Lu, Y. Zhu and Y. Xia, *Science*, 2009, **324**, 1302–1305.
- L. Qu, Y. Liu, J.-B. Baek and L. Dai, *ACS Nano*, 2010, **4**, 1321–1326.
- J. Liang, Y. Zheng, J. Chen, J. Liu, D. Hulicova-Jurcakova, M. Jaroniec and S. Z. Qiao, *Angew. Chem., Int. Ed.*, 2012, **51**, 3892–3896.
- R. Liu, D. Wu, X. Feng and K. Müllen, *Angew. Chem., Int. Ed.*, 2010, **49**, 2565–2569.
- H. Wang, Y. Liang, Y. Li and H. Dai, *Angew. Chem., Int. Ed.*, 2011, **50**, 10969–10972.
- S. Guo and S. Sun, *J. Am. Chem. Soc.*, 2012, **134**, 2492–2495.
- M. Jahan, Q. Bao and K. P. Loh, *J. Am. Chem. Soc.*, 2012, **134**, 6707–6713.
- R. Bashyam and P. Zelenay, *Nature*, 2006, **443**, 63–66.
- E. Proietti, F. Jaouen, M. Lefèvre, N. Larouche, J. Tian, J. Herranz and J.-P. Dodelet, *Nat. Commun.*, 2011, **2**, 416.
- Y. Liang, Y. Li, H. Wang, J. Zhou, J. Wang, T. Regier and H. Dai, *Nat. Mater.*, 2011, **10**, 780–786.
- Y. Li, W. Zhou, H. Wang, L. Xie, Y. Liang, F. Wei, J.-C. Idrobo, S. J. Pennycook and H. Dai, *Nat. Nanotechnol.*, 2012, **7**, 394–400.
- K. Gong, F. Du, Z. Xia, M. Durstock and L. Dai, *Science*, 2009, **323**, 760–764.
- M. Lefèvre, E. Proietti, F. Jaouen and J.-P. Dodelet, *Science*, 2009, **324**, 71–74.
- G. Wu, K. L. More, C. M. Johnston and P. Zelenay, *Science*, 2011, **332**, 443–447.
- Z.-H. Sheng, L. Shao, J.-J. Chen, W.-J. Bao, F.-B. Wang and X.-H. Xia, *ACS Nano*, 2011, **5**, 4350–4358.
- Z. Wang, R. Jia, J. Zheng, J. Zhao, L. Li, J. Song and Z. Zhu, *ACS Nano*, 2011, **5**, 1677–1684.
- W. Yang, T.-P. Fellingner and M. Antonietti, *J. Am. Chem. Soc.*, 2010, **133**, 206–209.
- S. Wang, D. Yu, L. Dai, D. W. Chang and J.-B. Baek, *ACS Nano*, 2011, **5**, 6202–6209.
- S. Wang, D. Yu and L. Dai, *J. Am. Chem. Soc.*, 2011, **133**, 5182–5185.
- J.-S. Lee, T. Lee, H.-K. Song, J. Cho and B.-S. Kim, *Energy Environ. Sci.*, 2011, **4**, 4148–4154.
- W. S. Hummers Jr and R. E. Offeman, *J. Am. Chem. Soc.*, 1958, **80**, 1339.

- 38 D. Li, M. B. Müller, S. Gilje, R. B. Kaner and G. G. Wallace, *Nat. Nanotechnol.*, 2008, **3**, 101–105.
- 39 S. Stankovich, D. A. Dikin, R. D. Piner, K. A. Kohlhaas, A. Kleinhammes, Y. Jia, Y. Wu, S. T. Nguyen and R. S. Ruoff, *Carbon*, 2007, **45**, 1558–1565.
- 40 S. Stankovich, R. D. Piner, X. Chen, N. Wu, S. T. Nguyen and R. S. Ruoff, *J. Mater. Chem.*, 2006, **16**, 155–158.
- 41 S. Stankovich, D. A. Dikin, G. H. B. Dommett, K. M. Kohlhaas, E. J. Zimney, E. A. Stach, R. D. Piner, S. T. Nguyen and R. S. Ruoff, *Nature*, 2006, **442**, 282–286.
- 42 W. Xiong, F. Du, Y. Liu, A. Perez Jr, M. Supp, T. S. Ramakrishnan, L. Dai and L. Jiang, *J. Am. Chem. Soc.*, 2010, **132**, 15839–15841.